The Astrophysical Journal, 893:62 (9pp), 2020 April 10 https://doi.org/10.3847/1538-4357/ab7d3d
© 2020. The American Astronomical Society. All rights reserved.

Higher Radial Harmonics of Sausage Oscillations in Coronal Loops

Daye Lim[1,2], Valery M. Nakariakov[1,3], Dae Jung Yu[1,2], Il-Hyun Cho[2], and Yong-Jae Moon[1,2]
[1] School of Space Research, Kyung Hee University, 1732, Deogyeong-daero, Giheung-gu, Yongin-si, Gyeonggi-do 17104, Republic of Korea; V.Nakariakov@warwick.ac.uk
[2] Department of Astronomy and Space Science, Kyung Hee University, 1732, Deogyeong-daero, Giheung-gu, Yongin-si, Gyeonggi-do 17104, Republic of Korea
[3] Centre for Fusion, Space and Astrophysics, Department of Physics, University of Warwick, Coventry CV4 7AL, UK
Received 2020 February 5; revised 2020 March 3; accepted 2020 March 4; published 2020 April 15

Abstract

Impulsively excited sausage oscillations of a plasma cylinder with a smooth radial profile of Alfvén speed are analyzed with a numerical solution of the initial-value problem for a partial differential equation of the Klein–Gordon type, describing linear magnetoacoustic oscillations with a fixed axial wavelength and an azimuthal mode number. The range of analyzed ratios of Alfvén speeds outside and inside the cylinder is from 2 to 10. Both trapped and leaky regimes of the oscillations are considered. It is shown that even in the long-wavelength limit, i.e., for axial wavenumbers much smaller than the cutoff values, damping times of higher radial sausage harmonics could be significantly greater than the oscillation periods, i.e., several oscillation cycles could be present in the signal. The quality factors decrease with decfreasing ratios of Alfvén speeds outside and inside the cylinder. Oscillation periods of the second and third radial harmonics remain practically independent of the axial wavelength even when the wavelength is shorter than the radius of the cylinder. The ratios of oscillation periods of fundamental and higher radial and axial harmonics are found to be significantly different, up to a factor of two in the long-wavelength limit. It is concluded that higher radial harmonics could be responsible for the departure of observed sausage oscillation signals from a harmonic shape, especially during the first several cycles of the oscillation. Even in the absence of spatially resolved data, higher axial and radial harmonics can be distinguished from each other by the period ratios.

Unified Astronomy Thesaurus concepts: Solar flares (1496); Solar oscillations (1515); Magnetohydrodynamics (1964)

1. Introduction

Solar flare emissions commonly show flux variations called quasi-periodic pulsations (QPPs). QPPs have been observed in a wide range of wavelengths from radio to gamma-rays (see, e.g., Nakariakov & Melnikov 2009; Van Doorsselaere et al. 2016; McLaughlin et al. 2018, for comprehensive reviews). In solar flares the period of QPPs ranges from sub-seconds to a few tens of minutes, while in longer stellar flares the QPP period can reach one hour or longer (e.g., Pugh et al. 2016). It has become clear that QPPs are a common and possibly intrinsic feature of flares (Kupriyanova et al. 2010; Simões et al. 2015; Inglis et al. 2016). Various mechanisms of QPPs have been suggested (Van Doorsselaere et al. 2016; McLaughlin et al. 2018), with two major categories comprising magnetohydrodynamics (MHD) oscillations and repetitive regimes of magnetic reconnection (magnetic dripping). However, other options remain open. One interesting feature of QPPs is the often detected anharmonic modulation patterns, i.e., the shape of the oscillatory signal could be different from the harmonic one (Nakariakov et al. 2019). Possible mechanisms responsible for the anharmonic signal are the coalescence instability of two coronal loops (Tajima et al. 1987; Kolotkov et al. 2016), MHD auto-oscillations (Nakariakov et al. 2010) and the superposition of several different oscillation modes (e.g., Van Doorsselaere et al. 2011; Kupriyanova et al. 2013; Kolotkov et al. 2015).

Theoretical models describing MHD oscillations, which have been used for interpretation of QPPs, are usually based on the consideration of standing perturbations of a straight magnetic cylinder or a slab that represents the flaring loop (e.g., Rosenberg 1970; Zajtsev & Stepanov 1975; Edwin & Roberts 1983). Properties of different MHD modes are determined by a set of three mode numbers that describe the mode structure in the radial, azimuthal, and axial directions. The axisymmetric fast magnetoacoustic mode, with the azimuthal number $m = 0$, is called a sausage mode. This mode is also known as "radial" or "peristaltic." The need to satisfy the line-tying boundary conditions at the photospheric footpoints of the oscillating loop introduces the axial wavenumber k_z. The axial mode number is the number of axial half-wavelengths along the loop. The wave with the lowest axial mode number is called the fundamental, or global mode (Nakariakov et al. 2003). The number of nodes in the radial structure of the radial velocity in a sausage oscillation determines the radial wavenumber.

In observations, sausage modes appear to be responsible for QPPs the periods ranging from a fraction of a second up to a minute (e.g., Van Doorsselaere et al. 2016), which is usually detected in the non-thermal emission. In particular, Nakariakov et al. (2003) interpreted 4–17 s QPPs of the gyrosynchrotron emission in a solar flare, as a fundamental sausage harmonic. Van Doorsselaere et al. (2011) associate 8.5 s QPP in the flaring chromospheric and coronal emission with a sausage oscillation. Su et al. (2012) interpreted sub-minute quasi-periodic variations of the EUV intensity with sausage oscillations. Yu et al. (2013) demonstrated that 1 s wiggles of zebra patterns in the dynamic spectra of the radio emission generated by a flare could be produced by a sausage oscillation. Tian et al. (2016) interpreted 25 s oscillations of the intensity and Doppler shift of the Fe XXI in a flare as a sausage oscillation. The observed quarter-period phase shift between the Doppler shift and intensity oscillations strengthens this interpretation. Mészárosová et al. (2016) found signatures of sausage oscillations with characteristic periods of 0.7 s and 2 s

in the broadband microwave emission around 1 GHz. Recently, Carley et al. (2019) suggested that 2.3 s QPPs of a 228 MHz radio source in a flare were caused by a sausage oscillation, too. Similar periodicities have been detected in the lightcurves of stellar flares, suggesting that sausage oscillations could be present there as well (e.g., Zaitsev et al. 2004; Contadakis et al. 2004, 2012; Tsap et al. 2011; Doyle et al. 2018).

Sausage modes occur in two regimes: the trapped regime, when the oscillations are evanescent outside the oscillating plasma cylinder, and the leaky regime, when the energy is radiated outward (or "leak") in the form of fast magnetoacoustic waves (e.g., Cally 1986; Vasheghani Farahani et al. 2014). The two regimes are separated by the cutoff axial wavelength. Sausage oscillations with an axial wavelength longer than the cutoff wavelength are subject to damping by leakage, i.e., the plasma cylinder acts in this regime as a fast magnetoacoustic antenna. The effectiveness of the wave damping caused by the leakage is not necessarily high, and the oscillation may be detectable for several oscillation cycles. In this case, leaky sausage oscillations could be responsible for observed QPP, and should not be excluded from consideration (Nakariakov et al. 2012). The cutoff wavelength of the fundamental radial harmonic has a finite value in cylinders with a straight, untwisted magnetic field inside and outside the cylinder, and a steep density profile (Edwin & Roberts 1983; Nakariakov et al. 2012). However, the fundamental radial harmonic can be trapped for all values of the axial wavelength in a twisted magnetic cylinder (e.g., Mikhalyaev 2005; Khongorova et al. 2012; Lim et al. 2018; Lopin & Nagorny 2019). A similar effect can occur in cylinders with a sufficiently diffused radial profile of the fast speed (e.g., Lopin & Nagorny 2014, 2015). Higher radial harmonics always have a cutoff axial wavelength.

Cutoff values and periods of standing sausage oscillations are also affected by field-aligned flows in the loops (Li et al. 2013, 2014). In the leaky regime, the resonant period of the fundamental, i.e., corresponding to the lowest values of the axial and radial mode numbers, sausage mode is determined by the fast magnetoacoustic travel time across the cylinder, while in the trapped regime the period is determined by the fast magnetoacoustic travel time along the cylinder (Cally 1986; Kopylova et al. 2002; Nakariakov et al. 2012). Resonant periods of sausage oscillations are weakly affected by the plasma parameter β (Inglis et al. 2009; Chen et al. 2016), provided β is less than unity. The period depends strongly on the contrast of the plasma densities inside and outside the cylinder (e.g., Edwin & Roberts 1983; Kopylova et al. 2002; Nakariakov et al. 2012), and depends only weakly on the density profile steepness (Pascoe et al. 2007a; Chen et al. 2016) and its specific shape (Pascoe et al. 2007b; Chen et al. 2015a, 2015b). The non-uniformity of the plasma along the field, connected, for example, with the increase in the loop's cross section with height or stratification, and the loop curvature, affect the resonant period insignificantly (Pascoe et al. 2009; Pascoe & Nakariakov 2016). In theoretical modeling, attention is also paid to the manifestation of sausage oscillations in observations made with specific instruments, i.e., the forward modeling of observables (e.g., Gruszecki et al. 2012; Reznikova et al. 2014; Kuznetsov et al. 2015; Shi et al. 2019). This modeling is based on knowledge of the spatial structure of the oscillatory mode of interest. Sausage modes are considered a promising tool for the seismological diagnostics of the plasma and the magnetic field in the flaring regions (e.g., Nakariakov et al. 2003; Guo et al. 2016).

The fundamental radial harmonic of the sausage mode has the longest decay time, as higher radial harmonics are usually leaky. Possibly for that reason, higher radial harmonics have received very little attention. In particular, the excitation of high transverse harmonics of plasma slabs was considered in Terradas et al. (2005). The roots of the dispersion relations obtained by Zajtsev & Stepanov (1975) and Edwin & Roberts (1983) for a step-function plasma cylinder, corresponding to higher radial harmonics, were included in the analysis by Kopylova et al. (2007). But if the radial structure of the initial perturbation is different from the structure of the fundamental radial harmonic, higher radial harmonics could be readily excited. Terradas et al. (2007) demonstrated that short-living higher radial harmonics of a plasma cylinder with a step-function radial profile of the density are effectively excited by an impulsive initial perturbation with a Gaussian or oscillatory radial structure. As in dense and thick flaring loops, the lifetimes of high radial sausage harmonics could be sufficiently long (e.g., Nakariakov & Melnikov 2009) that they could contribute to the total signal detected as the QPP modulation of the flaring signal. The aim of this study is to investigate higher radial sausage harmonics of sausage oscillations. The plasma configuration of this study, which is a zero-β plasma cylinder with a radially non-uniform plasma density, penetrated by a uniform straight magnetic field, is the same as that in Nakariakov et al. (2012). Here, we perform a parametric study of the sausage oscillations, varying the spatial structure of the initial perturbation in order to excite higher radial harmonics. The paper is organized as follows. In Section 2, we present the model. Section 3 gives the results of sausage perturbation in each case. Conclusions are provided in Section 4

2. Model and Governing Equations

We consider sausage oscillations of a straight, axisymmetric, and longitudinally uniform magnetic flux tube of a circular cross section, filled in with a dense plasma, and surrounded by a plasma with a lower density, i.e., a plasma cylinder. Such a plasma configuration is penetrated by a straight uniform magnetic field $\boldsymbol{B}_0$, directed along the axis of the flux tube. The symmetry of the model suggests the use of the cylindrical coordinates r, ϕ, z, with the z-axis coinciding with the cylinder axis. Both the external and internal plasmas are taken to be of zero-β. The plasma density ρ_0 varies in the radial direction only. The equilibrium is reached by the lack of gradients of the total pressure and the magnetic tension force. The radial profile of the density has a maximum at the axis of the cylinder, at $r = 0$, and decreases smoothly in the radial direction. Thus, the Alfvén speed, $V_{\rm A}(r) = B_0\big/\sqrt{\mu_0\rho_0(r)}$, increases in the radial direction (see Figure 1 left). Specifically, the radial profile of the Alfvén speed is given by the expression

$$V_{\rm A} = V_{\rm Ae}\left[1 - \delta\exp\left(-\frac{r^\alpha}{a^\alpha}\right)\right], \tag{1}$$

where the parameters δ, α, and a are the depth, steepness and characteristic width of the profile, respectively. The parameter a could be considered as the effective radius of the modeled plasma cylinder. At the axis of the cylinder, the Alfvén speed is $V_{\rm Ai} = V_{\rm Ae}(1 - \delta)$. The Alfvén speed increases with the radial distance r, gradually approaching the value $V_{\rm Ae}$. We are not

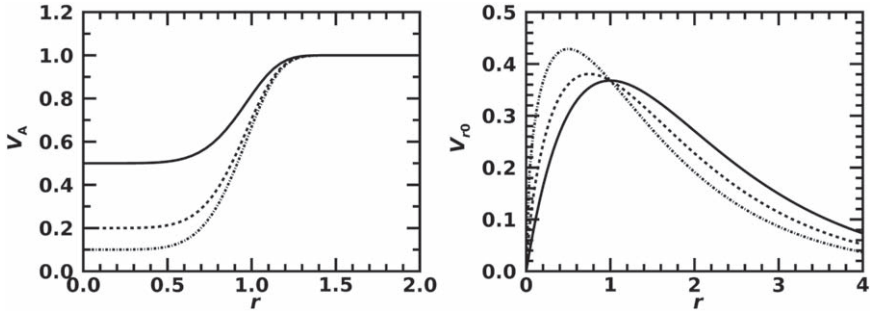

Figure 1. Left: examples of the radial profiles of the Alfvén speed in a plasma cylinder with different radial profiles of the plasma density. The solid curve corresponds to $V_{\rm Ae}/V_{\rm Ai} = 2$, the dashed curve to $V_{\rm Ae}/V_{\rm Ai} = 3$, and the dotted–dashed curve to $V_{\rm Ae}/V_{\rm Ai} = 10$. The Alfvén speed is normalized to its value at infinity, and the radial distance is normalized to the effective radius of the cylinder a. Right: the radial structure of the initial perturbation, v_{r0}. The solid curve corresponds to $\alpha = 1$, the dashed curve corresponds to $\alpha = 0.75$, and the dotted–dashed curve corresponds to $\alpha = 0.5$.

aware of an existing analytical solution for an eigenvalue problem with this profile. In the following, we restrict ourselves to the consideration of profiles with a fixed steepness, $\alpha = 6$.

The plasma and magnetic field perturbations are described by the MHD equations for an ideal cold (i.e., zero-β) plasma,

$$\frac{\partial \rho}{\partial t} = -\nabla \cdot (\rho \boldsymbol{v}), \tag{2}$$

$$\rho \frac{d\boldsymbol{v}}{dt} = \frac{1}{\mu_0}(\nabla \times \boldsymbol{B}) \times \boldsymbol{B}, \tag{3}$$

$$\frac{\partial \boldsymbol{B}}{\partial t} = \nabla \times (\boldsymbol{v} \times \boldsymbol{B}), \tag{4}$$

where ρ is the plasma density, $\boldsymbol{v} = (v_r, v_\phi, v_z)$ is the plasma velocity, $\boldsymbol{B} = (B_r, B_\phi, B_z)$ is the magnetic field, and μ_0 is the vacuum permeability.

In the following we restrict our attention to the perturbations characterized by alternate radial plasma flows, which are independent of the azimuthal angle ϕ, i.e., to sausage oscillations. As the equilibrium is uniform in the z-direction, we can take perturbations of all physical quantities to be proportional to $\cos(k_z z)$, i.e., making a Fourier transform in the z-direction. The parameter k_z is an axial wavenumber, i.e., the wavenumber along the axis of the cylinder. The choice for a specific value of k_z leads to the consideration of the corresponding single axial harmonic. In addition, we assume the perturbations to be linear, neglecting nonlinear terms. Then, Equations (2)–(4) reduce to the linearized fast magnetoacoustic wave equation for a fixed axial harmonic of the sausage perturbations of the plasma cylinder,

$$\frac{1}{V_{\rm A}^2(r)}\frac{\partial^2 v_r}{\partial t^2} + \left(k_z^2 + \frac{1}{r^2}\right)v_r - \frac{\partial^2 v_r}{\partial r^2} - \frac{1}{r}\frac{\partial v_r}{\partial r} = 0, \tag{5}$$

(see Nakariakov et al. 2012; Chen et al. 2015a, 2015b). Equation (5) is a cylindrical Klein–Gordon equation with a non-uniform speed.

Following the formalism described in Terradas et al. (2005), Nakariakov et al. (2012), and Hornsey et al. (2014), we study both trapped and leaky sausage oscillations as solutions to an initial-value problem. The boundary conditions in the radial direction are $v_r(r = 0, t) = v_r(r = 40a, t) = 0$. The boundary conditions are applied sufficiently far from the cylinder to allow for several cycles of sausage oscillations before the leaky perturbations reflected from the outer boundary return back to the cylinder and affect the oscillation. The variation of the axial wavenumber k_z allows us to excite sausage oscillations in both trapped and leaky regimes. The initial condition is given by the expression

$$v_r(r, t = 0) = v_{r0} = A_0 r^\alpha \exp\left(-\frac{r}{a}\right), \tag{6}$$

where A_0 is the amplitude, and the power index α controls the localization of the power in the cylinder. This form is independent of azimuthal angle ϕ and the radial velocity at the axis of the cylinder is zero, which correspond to sausage symmetry. Such an initial perturbation was found to be sufficiently different from radial eigenfunctions of profile (1), which allows us to excite simultaneously multiple radial harmonics. Thus, the discussed case is different from the case analyzed in Nakariakov et al. (2012), with preferential excitation of the fundamental radial harmonic. Varying $V_{\rm Ae}/V_{\rm Ai}$, we examine the dependence of the excited radial harmonics on the Alfvén speed contrast ratio (see Figure 1, left). The fixed value of k_z ensures that all excited harmonics are fundamental in the axial direction. Following Nakariakov et al. (2012) and Hornsey et al. (2014), we solve the initial-value problem constituted by Equation (5), supplemented by the initial and boundary conditions numerically, using the function *pdsolve* of the computing environment *Maple 2018.2*.

3. Results

The variation of the radial velocity in time after the excitation is obtained by taking the signal $V_r(t)$ at chosen radial positions, namely, at $r = 1.0a$, and in some cases at $0.5a$. Taking the signals at different radial distances is necessary to avoid analyzing the signal at a radial node of one of the radial harmonics. We employ the Fourier and Morlet wavelet transforms in the form introduced by Torrence & Compo (1998) for analyzing the signals.

3.1. Trapped and Leaky Regimes

The generated signals for sausage oscillations clearly show both leaky and trapped regimes; see Figures 2–4. Here, and throughout the paper this time is shown in units of $a/V_{\rm Ae}$. By order of magnitude, this time unit is about a second for a typical flaring loop with $a \approx 3$ Mm and $V_{\rm Ae} \approx 4\,{\rm Mm\,s^{-1}}$ (see, e.g., Nakariakov et al. 2003).

For an axial wavenumber $k_z a = 1.3$, the signal measured inside the cylinder exponentially decays (see Figure 2, top panel), corresponding to the leaky regime. For an axial

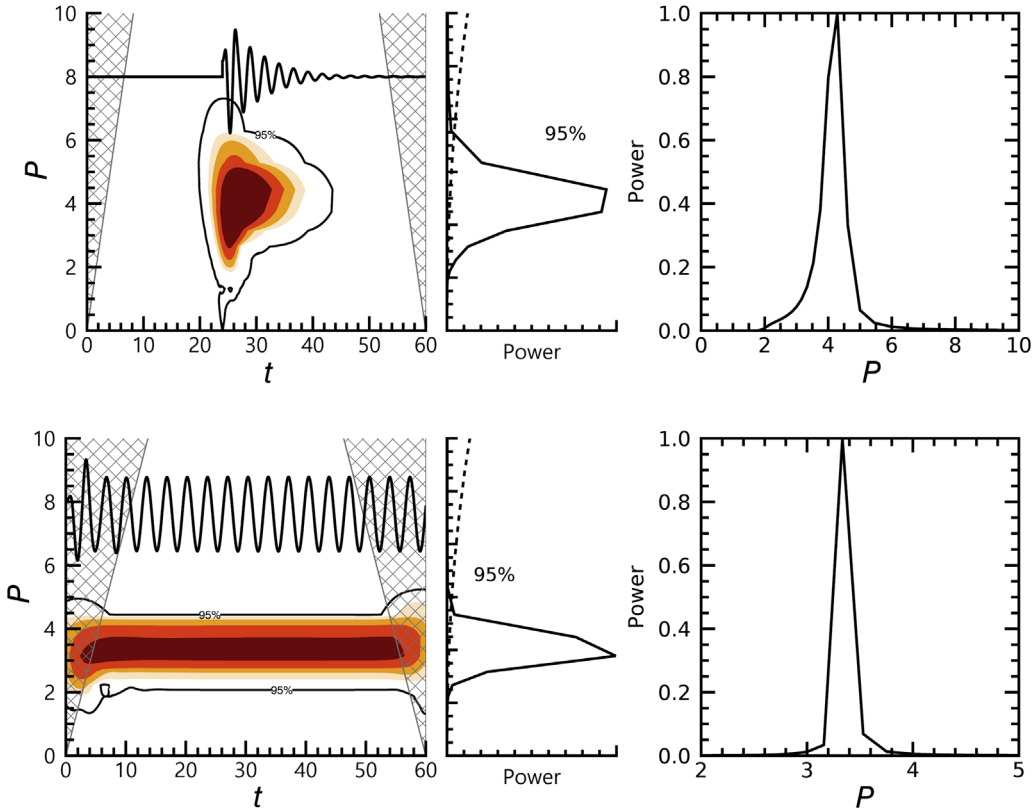

Figure 2. Leaky (top panel, with $k_z a = 1.3$) and trapped (bottom panel, with $k_z a = 2$) regimes of the sausage oscillation of a plasma cylinder with $V_{\rm Ae}/V_{\rm Ai} = 2$. The left column shows a radial velocity perturbation signal at $r = 0.5a$ and its Morlet wavelet spectrum. The solid contour shows the 95% significance level. The middle column shows the global wavelet power spectrum of the signal. The dashed line shows the 95% significance level. The right column shows the Fourier power spectrum of the signal. The Fourier power is normalized to the highest value.

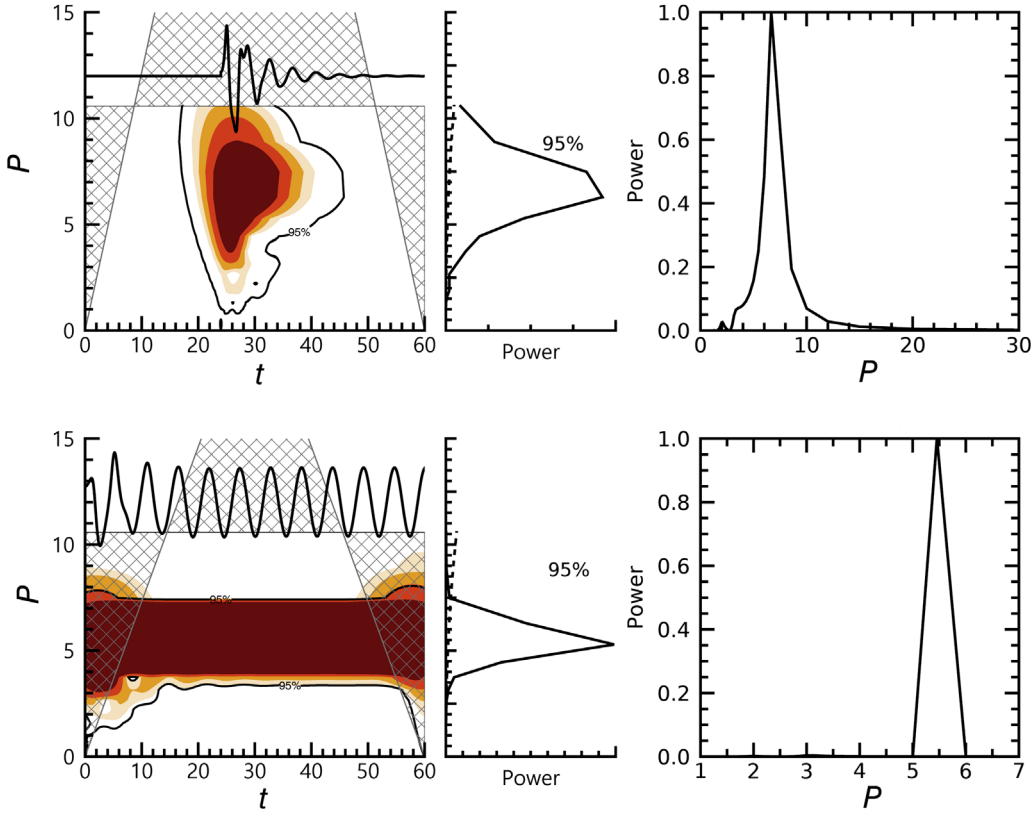

Figure 3. Same as Figure 2, but for $V_{\rm Ae}/V_{\rm Ai} = 3$, and $k_z a = 0.01$ (top) and $k_z a = 1.5$ (bottom).

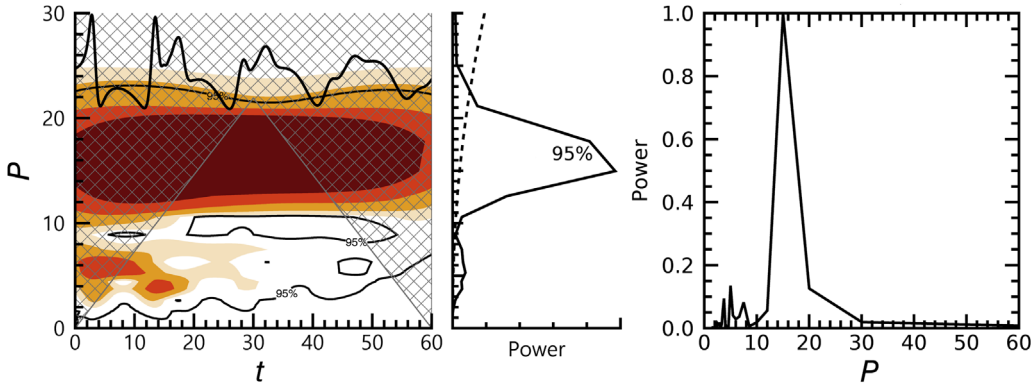

Figure 4. Highly anharmonic sausage oscillation with $k_z a = 0.01$, excited in a plasma cylinder with $V_{\rm Ae}/V_{\rm Ai} = 10$. The panels and notations are the same as in Figure 2.

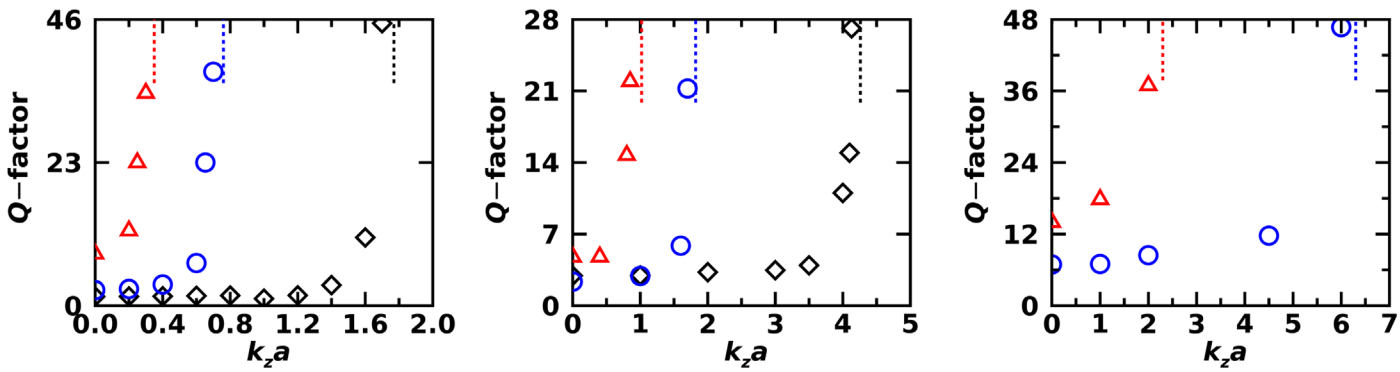

Figure 5. Quality factors of different radial harmonics of sausage oscillations in the leaky regime for different normalized axial wavenumbers. The left, middle, and right panels show the fundamental, second, and third harmonics, respectively. The red triangles correspond to $V_{\rm Ae}/V_{\rm Ai} = 10$, blue circles correspond to $V_{\rm Ae}/V_{\rm Ai} = 5$, and black diamonds correspond to $V_{\rm Ae}/V_{\rm Ai} = 2$. The vertical dashed lines show the corresponding cutoff values.

wavenumber $k_z a = 2$, the oscillation does not decay. It indicates that in those experiments the cutoff value of the axial wavenumber for the fundamental mode, which separates the leaky and trapped regimes, is between 1.3 and 2. Fundamental sausage oscillations with bigger values of $k_z a$ are trapped. Using the expression for the normalized cutoff axial wavenumber in a plasma cylinder with a step-function profile,

$$k_z^{\rm cutoff} a \approx 2.40\left(\frac{V_{\rm Ae}^2}{V_{\rm Ai}^2} - 1\right)^{-1/2} \tag{7}$$

(Edwin & Roberts 1983), we get $k_z^{\rm cutoff} a \approx 1.39$ for $V_{\rm Ae}/V_{\rm Ai} = 2$. This value is consistent with our finding.

In both regimes, both global wavelet and Fourier power spectra show the dominance of the fundamental harmonic. However, in the initial phase of the oscillation, there is a certain departure from a purely harmonic signal. It indicates that higher radial harmonics are also excited, but they leak out of the cylinder at a rate comparable with the oscillation period of the fundamental mode. The power of the high radial harmonics is too weak to be noticeable in the spectra.

Figure 5 (left panel) shows the dependence of quality factors of fundamental sausage harmonics in the leaky regime on the axial wavenumber. The quality factor is determined as the ratio of the oscillation damping time to the oscillation period. In all considered cases, the quality factor is greater than several units. For long wavelengths, i.e., for $k_z a \to 0$, the quality factor becomes weakly dependent on the axial wavenumber. When k_z approaches the cutoff value, the quality factors goes to infinity, as in the model there are no other wave damping mechanisms apart from the wave leakage.

3.2. Higher Radial Harmonics of Sausage Perturbations

Figure 6 demonstrates the effect of the radial structure of the driver given by Equation (6) shown in Figure 1 on the sausage oscillation. In all the cases, the signal shows some departure from the harmonic shape, which is manifested by the additional spectral peaks. The fundamental, second, and third harmonics have periods of about 16, 8, and 4 for all drivers. In the time domain, the change of the driver does not cause a significant modification of the signal shape. In the amplitude spectrum, this change is more pronounced. In particular, for the driver with $\alpha = 0.5$, the second harmonic is not effectively excited.

Figure 7 shows a multi-harmonic oscillatory signal excited by a broadband initial perturbation, and the three lowest radial harmonics of the signal. The harmonics were identified as distinct peaks in the power spectrum of the signal, and then filtered out by applying a Gaussian filter of the width about the width of the corresponding harmonic. The harmonics have consequently decreasing oscillation periods and amplitudes. The lifetimes of the second and third harmonics allow them to be present in the signal for up to three oscillation cycles of the fundamental harmonic. It is interesting that the quality factor of the third harmonic is apparently higher than that of the second one.

The middle and right panels of Figure 5 demonstrate that the quality factors of higher radial harmonics of the sausage mode in the leaky regime are higher than several units too. The

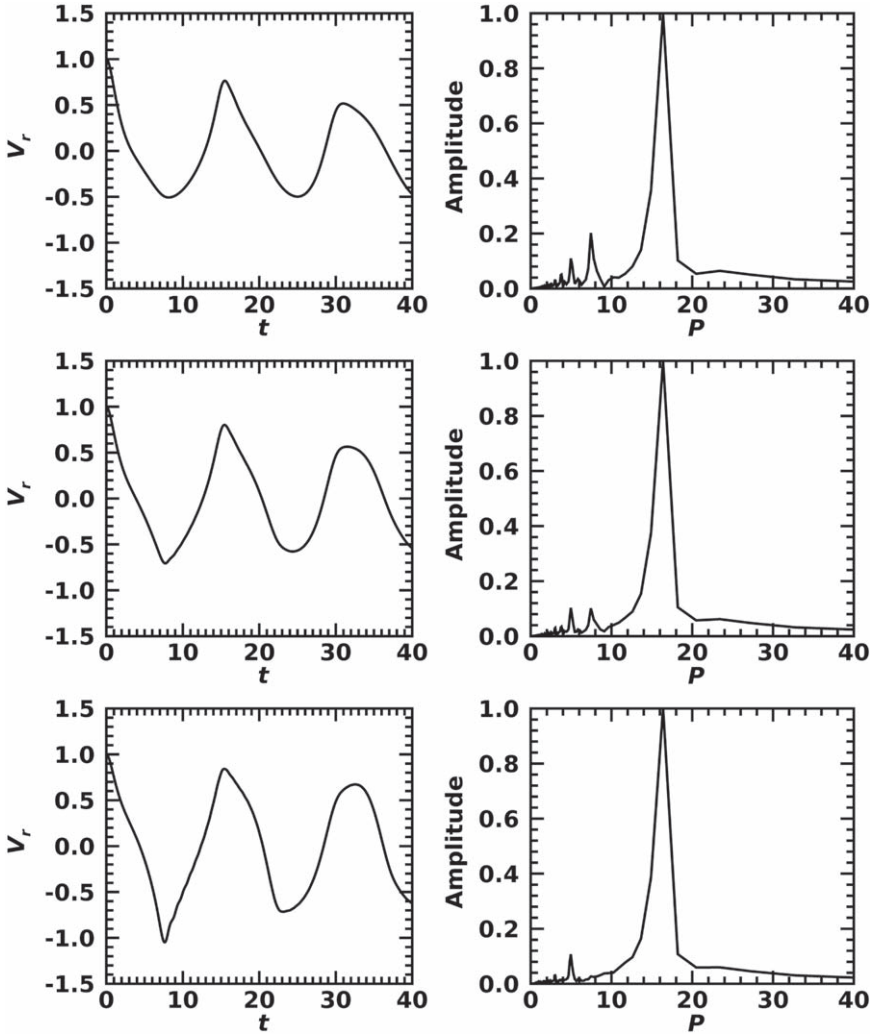

Figure 6. Effect of the initial driver on the shape (left column) and amplitude spectrum (right column) of the sausage oscillation signal with $k_z a = 0.1$ in a plasma cylinder with $V_{Ae}/V_{Ai} = 10$. The top row corresponds to $\alpha = 1$, the middle row corresponds to $\alpha = 0.75$, and the bottom corresponds to $\alpha = 0.5$. Both signals and spectra are normalized to the maximum values.

dependence of the quality factor of higher radial harmonics on the axial wavenumber is similar to the fundamental harmonic: the dependence decreases with decreasing axial wavenumber. This means that even when the axial wavenumber is much lower than the cutoff value, the damping time is still greater than the oscillation period. Also, as expected, in cylinders with higher density contrasts, the quality factors of leaky radial harmonics are higher. Cutoff values of the axial wavenumber grow with increasing the radial harmonic number, which is consistent with the well-known result obtained by Edwin & Roberts (1983) for a step-function plasma cylinder. The dependences shown in Figure 5 are similar to those shown in Figure 2 of Kopylova et al. (2007), obtained for a step-function cylinder.

The appearance of higher radial harmonics together with the fundamental harmonic, manifested by the departure of the signal shape from the harmonic in the initial stage of the oscillation, becomes more pronounced with increasing density contrast in the cylinder, i.e., the ratio V_{Ae}/V_{Ai}; see Figure 3. For a higher contrast, the leakage becomes less efficient, and the leaky modes can be detected in the cylinder at longer times. This result is consistent with the theoretical estimation of the quality factor of sausage oscillations, defined as the ratio of the damping time τ_{saus} and the oscillation period P_{saus},

$$\frac{\tau_{saus}}{P_{saus}} \propto \frac{V_{Ae}^2}{V_{Ai}^2}, \tag{8}$$

obtained in the long-wavelength limit for a plasma cylinder with a step-function density profile (Zajtsev & Stepanov 1975; Meerson et al. 1978); see also Lopin & Nagorny (2014). In the leaky regime, Figure 3 resembles Figure 3 of Terradas et al. (2007). For a higher contrast ratio $V_{Ae}/\ V_{Ai}$, even long-wavelength sausage oscillations can be highly anharmonic; see Figure 4.

Figure 8 shows the dependence of the oscillation periods of different radial harmonics on the axial wavenumber. In the leaky regime, for the axial wavenumbers smaller than the cutoff values, the oscillation periods are practically independent of the axial wavelength, which is consistent with the estimation made by Kopylova et al. (2007) in the long-wavelength limit for a step-function plasma cylinder. In the trapped regime, the fundamental harmonic period becomes dependent on the axial wavelength, as has been demonstrated in Nakariakov et al. (2003, 2012). However, the oscillation periods of the second and third radial harmonics remain practically independent of

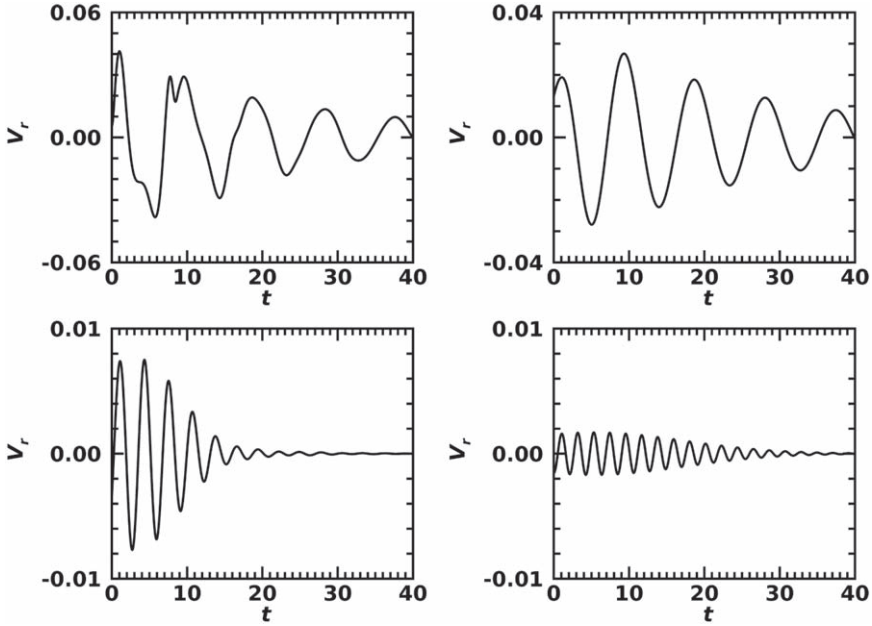

Figure 7. Top left: multi-harmonic sausage oscillation with $k_z a = 0.1$ in a plasma cylinder with $V_{\rm Ae}/V_{\rm Ai} = 5$ measured at $r = a$, and its harmonic composition: the fundamental (top right), second (bottom right), and third (bottom left) radial harmonics.

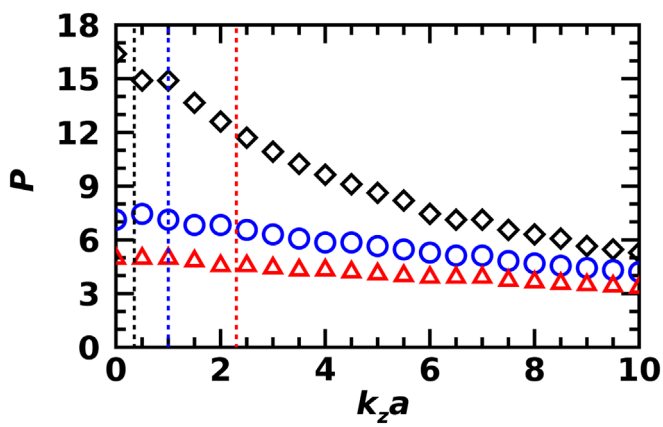

Figure 8. Dependence of sausage oscillation periods on the axial wavenumber in the three lowest radial harmonics of a plasma cylinder with $V_{\rm Ae}/V_{\rm Ai} = 10$. The fundamental radial harmonic is indicated by black diamonds; the second and third radial harmonics are represented by the blue circles and red triangles, respectively. The vertical dashed lines indicate the corresponding cutoff wavenumbers.

the wavelength even when the wavelength is shorter than the radius of the cylinder. Again, this result is similar to the result obtained for a step-function cylinder by Kopylova et al. (2007). Oscillation periods do not experience any noticeable change when the leaky regime changes to the trapped regime.

3.3. Oscillation-period Ratios

In oscillating coronal loops, the axial wavenumber k_z of standing sausage oscillations is discrete, and is prescribed by the loop length. One can introduce an axial (or parallel) mode number, n, which could be the number of parallel half-wavelengths along the loop. Thus, the fundamental parallel harmonic corresponds to $n = 1$, and has the axial wavenumber $k_z = \pi n/L$ where L is the loop length. Similarly, the radial harmonic number R can be introduced as the number of zeros in the radial velocity v_r dependence on r in the interval $r = [0, a]$, with $n = 1$ corresponding to the fundamental radial harmonic in which v_r has a single zero at the axis of the cylinder. The third "quantum" number, the azimuthal number m in all sausage harmonics, is the same, $m = 0$. Oscillation periods corresponding to different azimuthal, parallel, and radial harmonics could be labeled as P_{mnR}, with $P_{0n\rm R}$ describing sausage harmonics. In general, ratios of the oscillation periods corresponding to different harmonics are not integers (or multiplicative reciprocal). The departure of different axial harmonic period ratios P_{111}/nP_{1n1} from unity, e.g., caused by the axial non-uniformity of the oscillating loop, has been intensively studied as an important seismological observable. For the sausage mode, the values of P_{011}/nP_{0n1} and P_{011}/nP_{01n} have received less attention (e.g., Li et al. 2013), though they may also have a seismological potential.

Figure 9 shows the oscillation-period ratios of the lowest axial and radial sausage harmonics. In the calculation of P_{011}/nP_{0n1} the oscillation periods where taken at different values of $k_z a$, namely at $n\ k_z a$, while P_{011}/nP_{01n} was determined at the same $k_z a$. The ratios P_{011}/nP_{0n1} show a significant departure from unity, up to a factor of 2. The ratio P_{011}/nP_{0n1} is less than one, and approaches this value with increasing axial wavenumber. This effect should be attributed to the pronounced wave dispersion typical for the sausage mode in the vicinity of the cutoff axial wavenumber (see the discussion in Inglis & Nakariakov 2009). The behavior of the ratios P_{011}/nP_{01n} is different, as they are found to be around unity, and decrease with increasing axial wavenumber.

4. Conclusions

We analyzed impulsively excited sausage oscillations of a plasma cylinder, paying specific attention to different radial harmonics. The analysis was performed with a numerical solution of the initial-value problem for a partial differential equation of the Klein–Gordon type, describing linear magnetoacoustic oscillations with a fixed axial wavelength and an azimuthal mode number in a plasma cylinder with a smooth

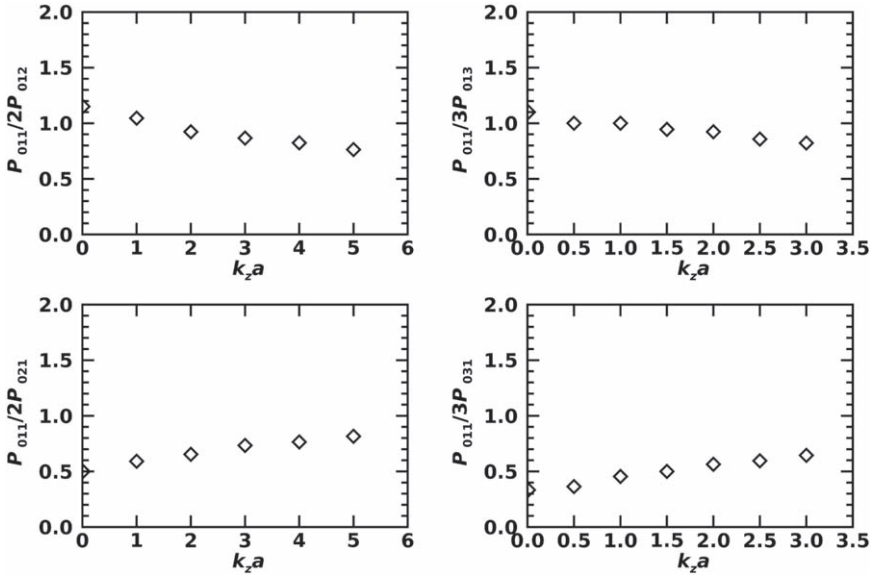

Figure 9. Ratios of oscillation periods of the fundamental radial harmonics to second and third radial and axial harmonics of the sausage mode on the axial wavenumber of the fundamental harmonics. The oscillation periods are labeled P_{mnR}, where the indices m, n, and R correspond to the azimuthal, axial, and radial harmonic numbers. In all the panels, the Alfvén speed contrast ratio is $V_{\rm Ae}/V_{\rm Ai} = 10$.

radial profile of Alfvén speed. Both trapped and leaky regimes of the oscillations were considered. Our findings are consistent with the results obtained for a step-function cylinder by asymptotic estimations (Zajtsev & Stepanov 1975; Meerson et al. 1978) and numerical determination of the complex roots of the transcendental algebraic equation describing dispersion relations (Kopylova et al. 2007).

Higher radial harmonics are found to be effectively excited by an initial pulse. The main result is that even in the long-wavelength limit, i.e., for the axial wavenumbers much smaller than the cutoff values, damping times of higher radial sausage harmonics could be significantly greater than the oscillation periods. This effect occurs even in plasma cylinders with low contrasts between the external and internal Alfvén speeds, e.g., about 2. The quality factors increase with increasing Alfvén speed (or density) contrast ratio inside and outside the cylinder. This means that if excited, sausage oscillations corresponding to higher radial harmonics could last in a coronal loop long enough to be detected. The periods of radial harmonics with the same k_z are independent of the specific radial shape of the initial perturbation. The specific partition of the energy between different radial harmonics depends on the driver. This effect is obvious, as it could be seen as a Fourier decomposition of the driver by natural radial harmonic functions. Oscillation periods of different radial harmonics are sufficiently different, i.e., by a factor of two or more. Hence, different radial harmonics are clearly distinguishable in observational data, provided the time resolution is several times shorter than the oscillation periods. We may estimate the required resolution. The oscillation period of fundamental sausage oscillations is about the transverse Alfvén travel time, i.e., about $a/V_{\rm Ai}$. For a flaring loop with a minor radius of about 5 Mm and internal Alfvén speed of about 0.5 Mm s^{-1}, the transverse Alfvén travel time is about 10 s (see, e.g., Van Doorsselaere et al. 2016).

The ratios of oscillation periods of higher radial and axial harmonics, P_{011}/nP_{01n} and P_{011}/nP_{0n1}, are found to be different. For example, in a cylinder with $V_{\rm Ae}/V_{\rm Ai} = 10$, for the fundamental harmonic axial wavenumbers from $k_z a = 0.01$ to $k_z a = 1$, we found $P_{011}/2P_{021} \approx 0.5$-0.6 and $P_{011}/2P_{012} = 1.1$–1.0. This range of axial wavenumbers corresponds to ratios of the loop length to diameter from 150 to 1.5, covers well the range of coronal loops observed in quiet-Sun and flaring active regions. The pronounced difference in P_{011}/nP_{0n1} and P_{011}/nP_{01n} allows for the discrimination of higher axial and radial harmonics in observations. The ratio $P_{011}/nP_{01n} \approx 1$ could also be due to nonlinear cascade, but this effect requires further study.

Detecting higher harmonics requires an oscillation-period resolution a few times shorter than this value, say, 3 s. As for a confident detection of a transient oscillation such as a QPP, one needs to have at least 5–6 measurements per oscillation cycle, and the required time resolution is about 0.5 s. Such a time resolution is readily achieved in the radio band. In the spatial domain, it is necessary to distinguish between the QPPs of emission from different segments of the oscillating loop, which requires an antenna beam size smaller than 10″–20″. In addition, the instruments must have a high sensitivity that allows detection of QPPs of weak amplitudes in the signal. This could be achieved at the Nobeyama Radioheliograph (e.g., Nakajima et al. 1994) and the Expanded Owens Valley Solar Array (e.g., Gary et al. 2018), and will be achievable at the upcoming Square Kilometre Array (e.g., Nakariakov et al. 2015).

Thus, higher radial spatial harmonics could be responsible for the appearance of statistically significant multiple spectral peaks in the analyzed signal, e.g., in QPPs of solar and stellar flare lightcurves, and the associated anharmonic shape of the oscillatory signal. In the time domain, higher radial harmonics could appear as anharmonic oscillatory patterns, which are often detected in QPP observations (e.g., Nakariakov et al. 2003, 2019; Van Doorsselaere et al. 2011), and, in particular, quasi-harmonic oscillations with subpeaks (e.g., Tajima et al. 1987). A similar effect could be caused by higher axial harmonics, i.e., harmonics with the same radial structure as the fundamental mode, but with an axial wavelength two times shorter. In both scenarios, shorter period components disappear gradually in the instantaneous or wavelet spectra of QPPs, i.e., with time the QPP signal becomes more harmonic. However,

the P_{011}/nP_{01n} ratios are about unity, while $P_{011}/nP_{0n1} < 1$. In the case of a nonlinear cascade, the shorter period signals should be gradually built up. The identification of whether the shorter period spectral components are associated with higher axial or radial harmonics is important for revealing the axial structure of the driver (not addressed in this study). For example, the oscillation-period ratios observed by Inglis & Nakariakov (2009), of about 0.75, indicate when the signal is likely a superposition of different axial harmonics of the oscillating loop, which is consistent with the interpretation proposed by the authors. On the other hand, the periods of 26 and 13 s detected by Kumar et al. (2017) are consistent with the coexistence of different radial harmonics. The periods of 1.43 and 0.83 s detected by Yu et al. (2013) seem to also favor the interpretation that there are different radial harmonics. However, a more rigorous analysis of each specific case requires accounting for all available information, which is out of the scope of this study.

This work was supported by the BK21 plus program through the National Research Foundation (NRF) funded by the Ministry of Education of Korea, the Basic Science Research Program through the NRF funded by the Ministry of Education (NRF-2016R1A2B4013131, NRF-2016R1A6A3A11932534, NRF-2019R1A2C1002634), NRF of Korea Grant funded by the Korean Government (NRF-2013M1A3A3A02042232), the Korea Astronomy and Space Science Institute under the R&D program supervised by the Ministry of Science, ICT and Future Planning, the Korea Astronomy and Space Science Institute under the R&D program, Development of a Solar Coronagraph on International Space Station (Project No. 2019-1-850-02) supervised by the Ministry of Science, ICT and Future Planning, and the Institute for Information & communications Technology Promotion (IITP) grant funded by the Korea government (MSIP) (2018-0-01422, Study on analysis and prediction technique of solar flares). V.M.N. acknowledges support from the STFC consolidated grant ST/P000320/1.

ORCID iDs

Daye Lim https://orcid.org/0000-0001-9914-9080
Valery M. Nakariakov https://orcid.org/0000-0001-6423-8286
Dae Jung Yu https://orcid.org/0000-0003-1459-3057
Il-Hyun Cho https://orcid.org/0000-0001-7514-8171
Yong-Jae Moon https://orcid.org/0000-0001-6216-6944

References

Cally, P. S. 1986, SoPh, 103, 277
Carley, E. P., Hayes, L. A., Murray, S. A., et al. 2019, NatCo, 10, 2276
Chen, S.-X., Li, B., Xia, L.-D., & Yu, H. 2015a, SoPh, 290, 2231
Chen, S.-X., Li, B., Xiong, M., Yu, H., & Guo, M.-Z. 2015b, ApJ, 812, 22
Chen, S.-X., Li, B., Xiong, M., Yu, H., & Guo, M.-Z. 2016, ApJ, 833, 114
Contadakis, M. E., Avgoloupis, S., Seiradakis, J., et al. 2004, AN, 325, 427
Contadakis, M. E., Avgoloupis, S. J., & Seiradakis, J. H. 2012, AN, 333, 583
Doyle, J. G., Shetye, J., Antonova, A. E., et al. 2018, MNRAS, 475, 2842
Edwin, P. M., & Roberts, B. 1983, SoPh, 88, 179
Gary, D. E., Chen, B., Dennis, B. R., et al. 2018, ApJ, 863, 83
Gruszecki, M., Nakariakov, V. M., & Van Doorsselaere, T. 2012, A&A, 543, A12
Guo, M.-Z., Chen, S.-X., Li, B., Xia, L.-D., & Yu, H. 2016, SoPh, 291, 877
Hornsey, C., Nakariakov, V. M., & Fludra, A. 2014, A&A, 567, A24
Inglis, A. R., Ireland, J., Dennis, B. R., Hayes, L., & Gallagher, P. 2016, ApJ, 833, 284
Inglis, A. R., & Nakariakov, V. M. 2009, A&A, 493, 259
Inglis, A. R., van Doorsselaere, T., Brady, C. S., & Nakariakov, V. M. 2009, A&A, 503, 569
Khongorova, O. V., Mikhalyaev, B. B., & Ruderman, M. S. 2012, SoPh, 280, 153
Kolotkov, D. Y., Nakariakov, V. M., Kupriyanova, E. G., Ratcliffe, H., & Shibasaki, K. 2015, A&A, 574, A53
Kolotkov, D. Y., Nakariakov, V. M., & Rowlands, G. 2016, PhRvE, 93, 053205
Kopylova, Y. G., Melnikov, A. V., Stepanov, A. V., Tsap, Y. T., & Goldvarg, T. B. 2007, AstL, 33, 706
Kopylova, Y. G., Stepanov, A. V., & Tsap, Y. T. 2002, AstL, 28, 783
Kumar, P., Nakariakov, V. M., & Cho, K.-S. 2017, ApJ, 836, 121
Kupriyanova, E. G., Melnikov, V. F., Nakariakov, V. M., & Shibasaki, K. 2010, SoPh, 267, 329
Kupriyanova, E. G., Melnikov, V. F., & Shibasaki, K. 2013, SoPh, 284, 559
Kuznetsov, A. A., Van Doorsselaere, T., & Reznikova, V. E. 2015, SoPh, 290, 1173
Li, B., Chen, S.-X., Xia, L.-D., & Yu, H. 2014, A&A, 568, A31
Li, B., Habbal, S. R., & Chen, Y. 2013, ApJ, 767, 169
Lim, D., Nakariakov, V. M., & Moon, Y.-J. 2018, JASTP, 175, 49
Lopin, I., & Nagorny, I. 2014, A&A, 572, A60
Lopin, I., & Nagorny, I. 2015, ApJ, 810, 87
Lopin, I., & Nagorny, I. 2019, ApJ, 882, 134
McLaughlin, J. A., Nakariakov, V. M., Dominique, M., Jelínek, P., & Takasao, S. 2018, SSRv, 214, 45
Meerson, B. I., Sasorov, P. V., & Stepanov, A. V. 1978, SoPh, 58, 165
Mészárosová, H., Rybák, J., Kashapova, L., et al. 2016, A&A, 593, A80
Mikhalyaev, B. B. 2005, AstL, 31, 406
Nakajima, H., Nishio, M., Enome, S., et al. 1994, IEEEP, 82, 705
Nakariakov, V., Bisi, M. M., Browning, P. K., et al. 2015, in Advancing Astrophysics with the Square Kilometre Array (AASKA14) (Trieste: SISSA), 169
Nakariakov, V. M., Hornsey, C., & Melnikov, V. F. 2012, ApJ, 761, 134
Nakariakov, V. M., Inglis, A. R., Zimovets, I. V., et al. 2010, PPCF, 52, 124009
Nakariakov, V. M., Kolotkov, D. Y., Kupriyanova, E. G., et al. 2019, PPCF, 61, 014024
Nakariakov, V. M., & Melnikov, V. F. 2009, SSRv, 149, 119
Nakariakov, V. M., Melnikov, V. F., & Reznikova, V. E. 2003, A&A, 412, L7
Pascoe, D. J., & Nakariakov, V. M. 2016, A&A, 593, A52
Pascoe, D. J., Nakariakov, V. M., & Arber, T. D. 2007a, A&A, 461, 1149
Pascoe, D. J., Nakariakov, V. M., & Arber, T. D. 2007b, SoPh, 246, 165
Pascoe, D. J., Nakariakov, V. M., Arber, T. D., & Murawski, K. 2009, A&A, 494, 1119
Pugh, C. E., Armstrong, D. J., Nakariakov, V. M., & Broomhall, A. M. 2016, MNRAS, 459, 3659
Reznikova, V. E., Antolin, P., & Van Doorsselaere, T. 2014, ApJ, 785, 86
Rosenberg, H. 1970, A&A, 9, 159
Shi, M., Li, B., Van Doorsselaere, T., Chen, S.-X., & Huang, Z. 2019, ApJ, 870, 99
Simões, P. J. A., Hudson, H. S., & Fletcher, L. 2015, SoPh, 290, 3625
Su, J. T., Shen, Y. D., Liu, Y., Liu, Y., & Mao, X. J. 2012, ApJ, 755, 113
Tajima, T., Sakai, J., Nakajima, H., et al. 1987, ApJ, 321, 1031
Terradas, J., Andries, J., & Goossens, M. 2007, SoPh, 246, 231
Terradas, J., Oliver, R., & Ballester, J. L. 2005, A&A, 441, 371
Tian, H., Young, P. R., Reeves, K. K., et al. 2016, ApJL, 823, L16
Torrence, C., & Compo, G. P. 1998, BAMS, 79, 61
Tsap, Y. T., Stepanov, A. V., Kopylova, Y. G., & Zhilyaev, B. E. 2011, AstL, 37, 49
Van Doorsselaere, T., De Groof, A., Zender, J., Berghmans, D., & Goossens, M. 2011, ApJ, 740, 90
Van Doorsselaere, T., Kupriyanova, E. G., & Yuan, D. 2016, SoPh, 291, 3143
Vasheghani Farahani, S., Hornsey, C., Van Doorsselaere, T., & Goossens, M. 2014, ApJ, 781, 92
Yu, S., Nakariakov, V. M., Selzer, L. A., Tan, B., & Yan, Y. 2013, ApJ, 777, 159
Zaitsev, V. V., Kislyakov, A. G., Stepanov, A. V., Kliem, B., & Furst, E. 2004, AstL, 30, 319
Zajtsev, V. V., & Stepanov, A. V. 1975, IGAFS, 37, 3